

# Vector meson spectral function in a dynamical AdS/QCD model

Yan-Qing Zhao<sup>1,\*</sup> and Defu Hou<sup>1,†</sup>

<sup>1</sup>*Institute of Particle Physics and Key Laboratory of Quark and Lepton Physics (MOS),  
Central China Normal University, Wuhan 430079, China*

(Dated: August 20, 2021)

## Abstract

By using gauge/gravity duality, we investigate the heavy vector meson dissociation with the presence of an intense magnetic field in a hot and dense medium. The results show that The dissociation of heavy quarkonium enhances as the magnetic field, chemical potential and temperature increase. The behavior of spectral functions is extraordinarily sensitive to temperature. With the increase of the medium temperature, the height of spectral function peak decreases rapidly. Most notably, the peak standing for  $J/\Psi$  will vanish showing the formation of free quarks when  $T > T_{max}(B|_{=0}, \mu|_{=0}) = 0.367 GeV \simeq 1.4T_c$ , which is consistent with the conclusion of lattice [1]. They pointed out the dissociation temperatures in the charmonium system is between  $1.1T_c$ (from  $F$  ansatz) and  $2.0T_c$ (from  $U$  ansatz). In addition, the findings also indicate that chemical potential has little effect on the spectral function peak for  $J/\Psi$  at vanishing magnetic field. However, the influence of chemical potential on the spectral function peak becomes more and more significant with the increase of magnetic field. Besides, we find the suppression is indeed stronger with the increase of mass of heavy meson. Finally, by introducing a dilaton, we show that the magnetic field has a stronger influence for the dissociation of heavy mesons when it is parallel to the polarization.

---

\* [zhaoyanqing@mails.ccnu.edu.cn](mailto:zhaoyanqing@mails.ccnu.edu.cn)

† Corresponding author; [houdf@mail.ccnu.edu.cn](mailto:houdf@mail.ccnu.edu.cn)

## I. INTRODUCTION

A new matter state, quark-gluon plasma, has been generated at the Relativistic Heavy-Ion Collider (RHIC) in Brookhaven. These substances are interconnected by strong interactions which can be elaborated by quantum chromodynamics (QCD). So this new state of matter is also extensively called the strongly-correlated quark-gluon plasma (sQGP) [2]. The strength of the coupling between them is related to the energy. At high energy, the coupling is very small, and quarks have the property of asymptotic freedom, which can be studied by perturbation theory. At low energy, the coupling is very large, and quarks have the property of color confinement, so the perturbation theory is no longer applicable and a non-perturbation method needs to be employed. Fortunately, gauge/gravity correspondence or the bulk/boundary correspondence [3–16], a new approach, provides a powerful tool to study the non-perturbative regime of the physic system. The most attractive achievement from the gauge/gravity correspondence is that one can also perform analytical calculation by this technique.

The suppression of  $J/\Psi$  and  $\Upsilon(1S)$  peaks in the dilepton spectrum plays an important role in many signals of phase transition. Heavy quarkonium may survive, due to Coulomb attraction between quark and antiquark, as bound states when the quark matter encounter phase transitions. By analysing the spectral functions in the Nambu-Jona-Lasinio model, Ref. [17] points out that quark-antiquark excitations, small mass and narrow width in the  $\pi - \sigma$  channels, still exist at  $T > T_c$  where  $T_c$  is the phase transition temperature. However, Ref. [18] studies  $J/\Psi$  and  $\eta_c$ , by discussing the correlation functions of  $J/\Psi$  at finite temperature on  $32^3 * (32 - 96)$  anisotropic lattices using the maximum entropy method (MEM), in the deconfined plasma from lattice QCD, the results show that  $J/\Psi$  and  $\eta_c$  can survives in the plasma with obvious resonance state up to  $T \simeq 1.6T_c$  and dissociate at  $1.6T_c \leq T \leq 1.9T_c$ . Next, Ref. [19] considers the  $Q\bar{Q}$  with quark masses close to the charm mass on very fine isotropic lattices, the results show that the  $J/\Psi$  and  $\eta_c$  can survive up to  $1.5T_c$  and vanish at  $3T_c$ .

RHIC experiments show that sQGP not only has the properties of high temperature and density, but also a very intense magnetic field engendered in noncentral relativistic heavy ion collision and exists long enough to also affect the produced quark-gluon plasma [20–28]. In recent years, a lot of work has revealed the dependence of thermal QGP properties on magnetic field and chemical potential [29–55]. Ref. [56] deliberates the finite-temperature influences on the spectral function in the vector channel and pointed out that the dissociation of the heavy vector meson tower onto

the AdS black hole results in the in-medium mass shift and the width broadening. The lattice QCD studies, for the  $J/\psi$  spectral functions at finite temperature, show that mesons can survive beyond  $2T_c$  where  $T_c$  denotes the phase transition temperature [18, 19, 57]. The paper [58], by introducing the probe D7-branes to the 10d gravitational backgrounds to add flavor degrees of freedom, indicates that the magnetic field decreases the mass gap of the meson spectrum along with their masses. Ref. [48] displays the heavy meson dissociation in a plasma with magnetic fields and states clearly the dissociation effect increases with the magnetic field for magnetic fields parallel and perpendicular, respectively, to the polarization. The case of finite density is studied in [59], which gives that increasing temperature and chemical potential decrease the peak of spectral functions showing the thermal dissociation process. Ref. [60] calculates the dissociation temperature of  $J/\psi$  and  $\Upsilon(1S)$  state by solving the Schrödinger equation of the potential model. They find the ratios of the dissociation temperatures for quarkonium with the  $U$ -ansatz of the potential to the deconfinement temperature to agree with the lattice results within a factor of two.

Inspired by [48, 59], the main objective of this manuscript is to investigate the spectral functions for  $J/\psi$  and  $\Upsilon(1S)$  state by considering a more general situation, including chemical potential and magnetic field in gravity background, which could better simulate the sQGP environment produced by RHIC experiments. The introduced magnetic field breaks the  $SO(3)$  invariance into  $SO(2)$  invariance, that is, the magnetic field only changes the geometry perpendicular to it which is different from other models. The manuscript is organized as follows. In section II, we review the magnetized holographic QCD model with running dilaton and chemical potential. In section III, we give the specific derivation process for calculating the spectral functions of  $J/\psi$  and  $\Upsilon(1S)$  state. In section IV, we show and discuss the figure results. Finally, this work is finished by summarizing the results and discussing some issues in section V.

## II. HOLOGRAPHIC QCD MODEL

We consider a 5d EMD gravity system with two Maxwell fields and a neutral dilatonic scalar field as a thermal background for the corresponding QCD. The Lagrangian is given as

$$\mathcal{L} = \frac{g_1(\phi)}{4} F_{(1)\mu\nu} F^{\mu\nu} + \frac{g_2(\phi)}{4} F_{(2)\mu\nu} F^{\mu\nu} + \frac{1}{2} \partial_\mu \phi \partial^\mu \phi + V(\phi). \quad (1)$$

where  $F_{(i)\mu\nu}$  ( $i = 1, 2$ ) is the field strength tensor for U(1) gauge field,  $g_i(\phi)$  ( $i = 1, 2$ ) is the gauge coupling kinetic function,  $\phi$  is the dilaton field.  $V(\phi)$  is the potential of the  $\phi$ , which

is closely related to on the scale function  $A(z)$ . By introducing external magnetic field in  $x_1$  direction damages the  $SO(3)$  invariance to  $SO(2)$  invariance in boundary spatial coordinates, so we consider the following anisotropic ansatz for the background blackening metric  $f_{\mu\nu}$  and  $(\phi, A_\mu)$  fields in Einstein frame [61]

$$g_{\mu\nu}dx^\mu dx^\nu = \frac{R^2 S(z)}{z^2}(-f(z)dt^2 + dx_1^2 + e^{B^2 z^2}(dx_2^2 + dx_3^2) + \frac{1}{f(z)}dz^2),$$

$$\phi = \phi(z), \quad A_{(1)\mu} = A_t(z)\delta_\mu^t, \quad F_{(2)\mu\nu} = Bdx_2 \wedge dx_3, \quad (2)$$

with

$$f(z) = 1 + \int_0^z d\xi \xi^3 e^{-B^2 \xi^2 - 3A(\xi)} [K + \frac{\tilde{\mu}^2}{2cR^2} e^{c\xi^2}],$$

$$K = -\frac{1 + \frac{\tilde{\mu}^2}{2cR^2} \int_0^{z_h} d\xi \xi^3 e^{-B^2 \xi^2 - 3A(\xi) + c\xi^2}}{\int_0^{z_h} d\xi \xi^3 e^{-B^2 \xi^2 - 3A(\xi)}},$$

$$\tilde{\mu} = \frac{\mu}{\int_0^{z_h} d\xi \frac{\xi e^{-B^2 \xi^2}}{g_1(\xi) \sqrt{S(\xi)}}}, \quad (3)$$

where  $R$  is the radius of the asymptotic AdS spaces,  $S(z)$  is the scale factor,  $f(z)$  represents the blackening function and  $\mu$  is the chemical potential. We stipulate that the asymptotic boundary is at  $z = 0$  and  $z = z_h$  labels the location of horizon where  $f(z_h) = 0$ . The concrete form of gauge coupling function  $g_1$  can be determined by fitting the vector meson mass spectrum. The linear Regge trajectories for  $B = 0$  can be restored when

$$g_1(z) = \frac{e^{-R_{gg} z^2 - B^2 z^2}}{\sqrt{S(z)}}. \quad (4)$$

Using  $S(z) = e^{2A(z)}$ , one can obtain  $R_{gg} = 1.16 GeV^2$  for heavy meson state  $J/\psi$ . In the following calculation, we take  $A(z) = -az^2$  where  $a = 0.15 GeV^2$  matching with the lattice QCD deconfinement temperature at  $B = 0 GeV^2$  [62].

The Hawking temperature with magnetic field and chemical potential can be computed by surface gravity

$$T(z_h, \mu, B) = \frac{-z_h^3 e^{-3A(z_h) - B^2 z_h^2}}{4\pi} (K + \frac{\tilde{\mu}^2}{2cR^2} e^{cz_h^2}). \quad (5)$$

The original paper [61] assumes that the dilaton field  $\phi$  remains real everywhere in the bulk, which leads to magnetic field  $B \leq B_c \simeq 0.61 GeV^2$ .

### III. THE DERIVATION PROCESS FOR SPECTRAL FUNCTIONS

In this section, we will calculate the spectral function for  $J/\psi$  state and  $\Upsilon(1S)$  state by a phenomenological model proposed in Ref. [59]. The vector field  $A_m = (A_\mu, A_z)(\mu = 0, 1, 2, 3)$  is used to represent the heavy quarkonium, which is dual to the gauge theory current  $J^\mu = \bar{\Psi}\gamma^\mu\Psi$ . The standard Maxwell action takes the following form

$$S = \int d^4x dz \sqrt{-g} e^{-\phi(z)} \left[ -\frac{1}{4g_5^2} F_{mn} F^{mn} \right], \quad (6)$$

where  $F_{mn} = \partial_m A_n - \partial_n A_m$ .  $\phi(z)$  is a background scalar field including three energy parameters,

$$\phi(z) = \kappa^2 z^2 + Mz + \tanh\left(\frac{1}{Mz} - \frac{\kappa}{\sqrt{\Gamma}}\right). \quad (7)$$

where  $\kappa$  labels the quark mass,  $\Gamma$  is the string tension of the quark pair and  $M$  denotes a large mass related to the heavy quarkonium non-hadronic decay. There is a matrix element  $\langle 0 | J_\mu(0) | X(1S) \rangle = \epsilon_\mu f_n m_n$  ( $X$  shows the heavy mesons  $\Upsilon$  or  $\Psi$ ,  $\langle 0 |$  is the hadronic vacuum,  $J_\mu$  is the hadronic current and  $f_n$  indicates the decay constant) when the heavy vector mesons decays into leptons. The value of three energy parameters for charmonium and bottomonium in the scalar field, determined by fitting the spectrum of masses [48], are respectively:

$$\begin{aligned} \kappa_c &= 1.2 \text{ GeV}, & \sqrt{\Gamma_c} &= 0.55 \text{ GeV}, & M_c &= 2.2 \text{ GeV}, \\ \kappa_b &= 2.45 \text{ GeV}, & \sqrt{\Gamma_b} &= 1.55 \text{ GeV}, & M_b &= 6.2 \text{ GeV}. \end{aligned} \quad (8)$$

The spectral functions for  $J/\Psi$  state and  $\Upsilon(1S)$  state will be calculated with the help of the membrane paradigm [63]. The equation of motion obtained from Eq. (6) are as follows

$$\partial^m \left( \frac{\sqrt{-g}}{h(z)} F_{mn} \right) = 0. \quad (9)$$

For the  $z$ -foliation, the conjugate momentum of the gauge field  $A^\mu$  is given by the following formula:

$$j^\mu = \frac{\sqrt{-g}}{h(z)} F^{z\mu}. \quad (10)$$

Supposing plane wave solutions for  $A^\mu$  have nothing to do with the coordinates  $x - 2$  and  $x_3$  - in other words the plane wave propagates in the  $x_1$  direction. The equation of motion (9) can be split into two parts: longitudinal-the fluctuations along  $(t, x_1)$ ; transverse-fluctuations along

$n$	State	$M_{\text{exp}}(\text{MeV})$	model1(MeV)	model2(MeV)
1	$J/\Psi$	$3096.916 \pm 0.011$	3037.1	3510.7
2	$\Psi(2S)$	$3686.109 \pm 0.012$	4126.0	4082.2
3	$\Psi(3S)$	$4039 \pm 1$	4971.9	4523.2
4	$\Psi(4S)$	$4421 \pm 4$	5679.0	4890.8

TABLE I. Holographic masses for the Charmonium S-wave resonances. Experimental results are from PDG[64].

$n$	State	$M_{\text{exp}}(\text{MeV})$	model1(MeV)	model2(MeV)
1	$\Upsilon(1S)$	$9460.3 \pm 0.26$	7073.7	9196.0
2	$\Upsilon(2S)$	$10023.26 \pm 0.32$	9040.4	10276.6
3	$\Upsilon(3S)$	$10355.2 \pm 0.5$	10620.0	10645.9
4	$\Upsilon(4S)$	$10579.4 \pm 1.2$	11963.0	10951.9

TABLE II. Holographic masses for the Bottomonium S-wave resonances. Experimental results are from PDG[64].

$x_2, x_3$ . Combined with Eq.(10), the components  $t, x_1, z$  of Eq.(9) can be expressed respectively as

$$-\partial_z j^t + \frac{R\sqrt{S(z)}e^{Bz-\phi}}{zf(z)}\partial_{x_1}F_{x_1t} = 0, \quad (11)$$

$$-\partial_z j^{x_1} - \frac{R\sqrt{S(z)}e^{Bz-\phi}}{zf(z)}\partial_t F_{x_1t} = 0, \quad (12)$$

$$\partial_{x_1}j^{x_1} + \partial_t j^t = 0. \quad (13)$$

By using the Bianchi identity, one can get

$$\partial_z F_{x_1t} - \frac{ze^{\phi-Bz}}{R\sqrt{S(z)}f(z)}\partial_t j^z + \frac{zf(z)e^{\phi-Bz}}{R\sqrt{S(z)}}\partial_{x_1}j^t = 0. \quad (14)$$

The longitudinal "conductivity" and its derivative are defined as

$$\sigma_L(\omega, \vec{p}, z) = \frac{j^{x_1}(\omega, \vec{p}, z)}{F_{x_1t}(\omega, \vec{p}, z)}, \quad (15)$$

$$\partial_z \sigma_L(\omega, \vec{p}, z) = \frac{\partial_z j^{x_1}}{F_{x_1t}} - \frac{j^{x_1}}{F_{x_1t}^2}\partial_z F_{x_1t}. \quad (16)$$

The Kubo's formula shows that the five dimensional "conductivity" at the boundary is related to the retarded Green's function:

$$\sigma_L(\omega) = \frac{-G_R^L(\omega)}{i\omega}. \quad (17)$$

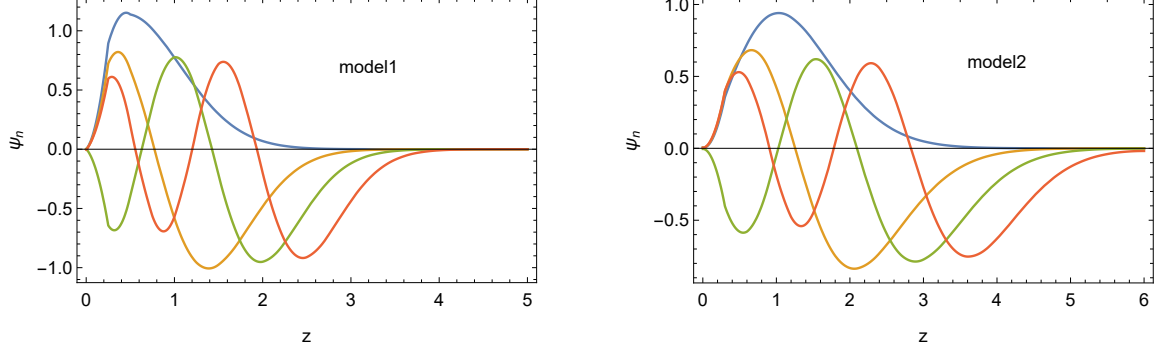


FIG. 1. The ground state and the first three excited bulk eigenmodes dual to charmonium. Left panel is from quadratic dilaton. Right panel is from nonquadratic dilaton.

where  $\sigma_L$  is interpreted as the longitudinal AC conductivity. By using Eq.(11), Eq.(13), Eq.(14) and the momentum  $P = (\omega, 0, 0, 0)$ , the Eq.(16) can be written as

$$\partial_z \sigma_L(\omega, z) = \frac{iz\omega}{f(z)e^{B^2 z^2 - \phi}} (\sigma(\omega, z)^2 - \frac{e^{2B^2 z^2 - 2\phi}}{z^2}). \quad (18)$$

The initial condition for solving the equation can be obtained by requiring regularity at the horizon  $\partial_z \sigma_L(\omega, z) = 0$ . The same procedure may be easily adapted to obtain the transverse AC conductivity

$$\partial_z \sigma_T(\omega, z) = \frac{iz\omega}{f(z)e^{-\phi}} (\sigma(\omega, z)^2 - \frac{e^{-2\phi}}{z^2}). \quad (19)$$

It is not difficult to find that the metric Eq.(2) restores the SO(3) invariance and the flow equations Eq.(18) and Eq.(19) have the same form when magnetic field  $B = 0$ . The spectral function is defined by the retarded Green's function

$$\rho(\omega) \equiv -Im G_R(\omega) = \omega Re \sigma(\omega, 0) \quad (20)$$

#### IV. RESULTS

With all the preparations in place, in this section the spectral functions for  $J/\Psi$  state and  $\Upsilon(1S)$  state will be given with polarization parallel and perpendicular to the magnetic field. Before that, we show the holographic quarkonium eigenfunctions, in Fig.1 and Fig.2, and masses, in tables I and II, for the states  $1S, 2S, 3S, 4S$  in two different dilaton, quadratic dilaton(model1)- $\phi(z) = \kappa^2 z^2 + Mz + \tanh(\frac{1}{Mz} - \frac{\kappa}{\sqrt{\Gamma}})$ , nonquadratic dilaton(model2) [65]- $\phi(z) = (\kappa z)^{2-\alpha} + Mz + \tanh(\frac{1}{Mz} - \frac{\kappa}{\sqrt{\Gamma}})$ .

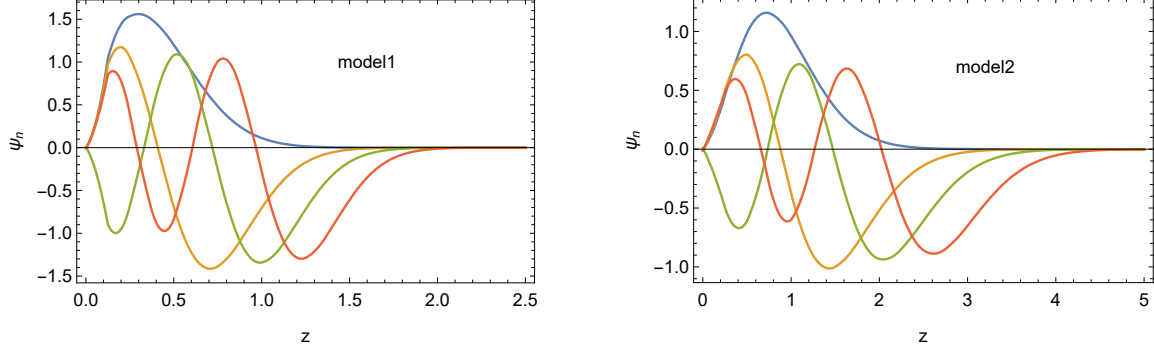


FIG. 2. The ground state and the first three excited bulk eigenmodes dual to bottomonium. Left panel is from quadratic dilaton. Right panel is from nonquadratic dilaton.

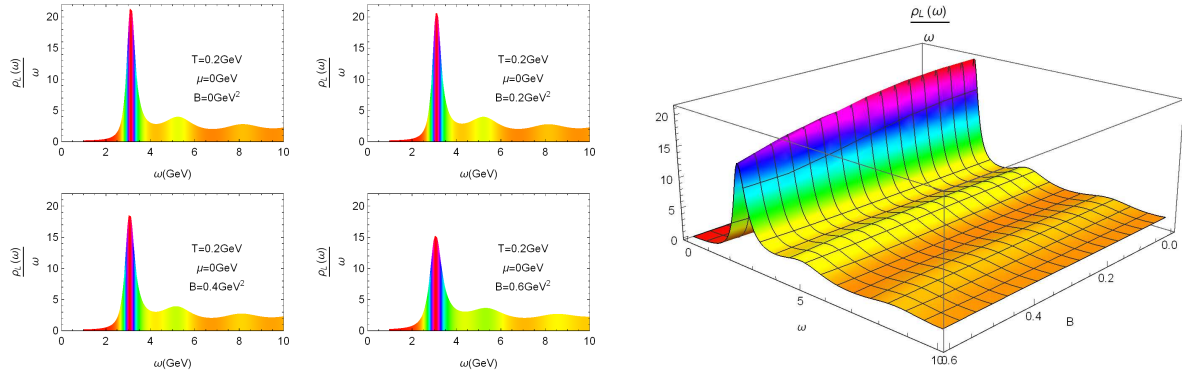


FIG. 3. The spectral functions of the  $J/\Psi$  state with different magnetic field  $B$  at  $T = 0.2\text{GeV}$  and  $\mu = 0\text{GeV}$ . The left picture, from left to right and from top to bottom, the values of the magnetic field are  $B = 0\text{GeV}^2$ ,  $B = 0.2\text{GeV}^2$ ,  $B = 0.4\text{GeV}^2$  and  $B = 0.6\text{GeV}^2$  respectively.

Further, we compare the theoretical values with the experimental values for heavy mesons mass. In Fig.3, the spectral functions of the  $J/\Psi$  state for different magnetic field parallel to the polarization in zero chemical potential are shown. One can find that increasing magnetic field reduces the height of the peak. In particularly, the change of the height of peak is not very significant at  $B \leq 0.3\text{GeV}^2$ . The height of the peak, however, decreases rapidly when  $B \geq 0.3\text{GeV}^2$ . The spectral functions of the  $J/\Psi$  state for different magnetic field parallel to the polarization in finite chemical potential are displayed in Fig.4. By comparing Fig.3 with Fig.4, one may discover that the effect of chemical potential on the spectral function for  $J/\Psi$  is not very notable.

In view of this phenomenon, we give the spectral functions of the  $J/\Psi$  state for different chemical potential in zero magnetic field and in finite magnetic field parallel to the polarization in Fig.5 and Fig.6 respectively. It can be seen from Fig.5 that in the absence of magnetic field, the effect of



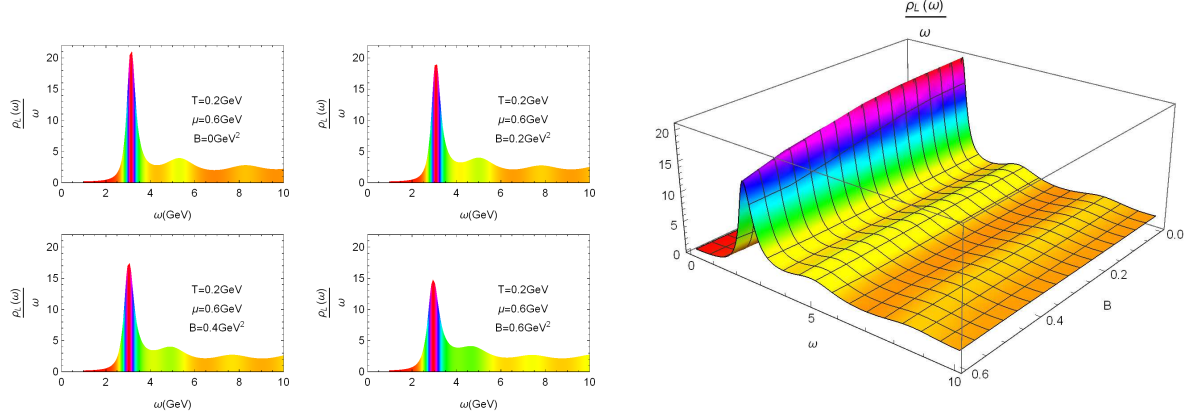


FIG. 4. The spectral functions of the  $J/\Psi$  state with different magnetic field  $B$  at  $T = 0.2\text{GeV}$  and  $\mu = 0.6\text{GeV}$ . The left picture, from left to right and from top to bottom, the values of the magnetic field are  $B = 0\text{GeV}^2$ ,  $B = 0.2\text{GeV}^2$ ,  $B = 0.4\text{GeV}^2$  and  $B = 0.6\text{GeV}^2$  respectively.

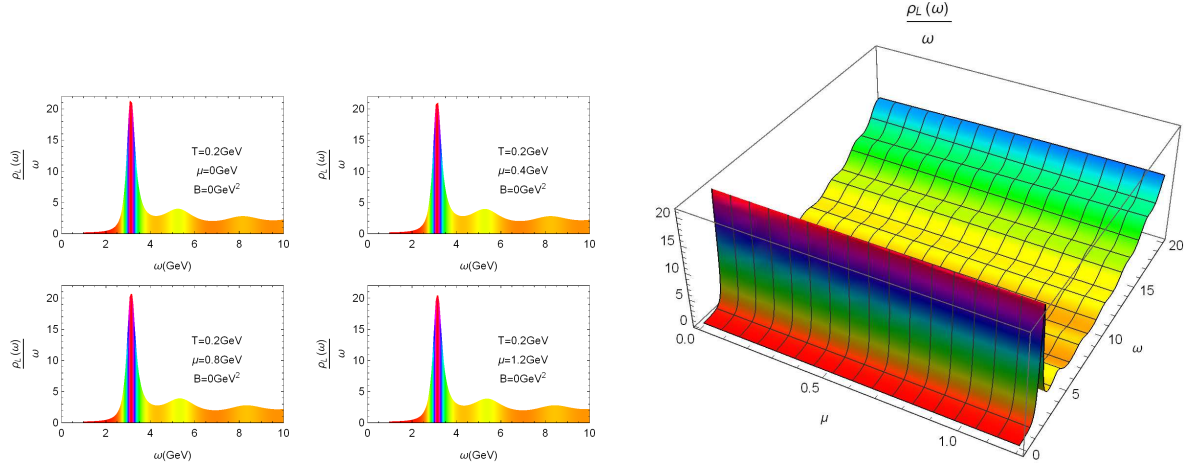


FIG. 5. The spectral functions of the  $J/\Psi$  state with different chemical potential  $\mu$  at  $T = 0.2\text{GeV}$  and  $B = 0\text{GeV}^2$ . The left picture, from left to right and from top to bottom, the values of the chemical potential are  $\mu = 0\text{GeV}$ ,  $\mu = 0.4\text{GeV}$ ,  $\mu = 0.8\text{GeV}$  and  $\mu = 1.2\text{GeV}$  respectively.

chemical potential on the height of the peak of spectral function can be ignored. To keep it going, now let's look at Fig.6, increasing chemical potential significantly reduces the height of the peak for finite magnetic field. An relatively general conclusion is obtained: both magnetic field and chemical potential tend to promote the melting of  $J/\Psi$ .

In Fig.7 and Fig.8, the behavior of spectral functions is extraordinarily sensitive to temperature of current physical system. With the increase of QGP temperature, the height of peak decreases

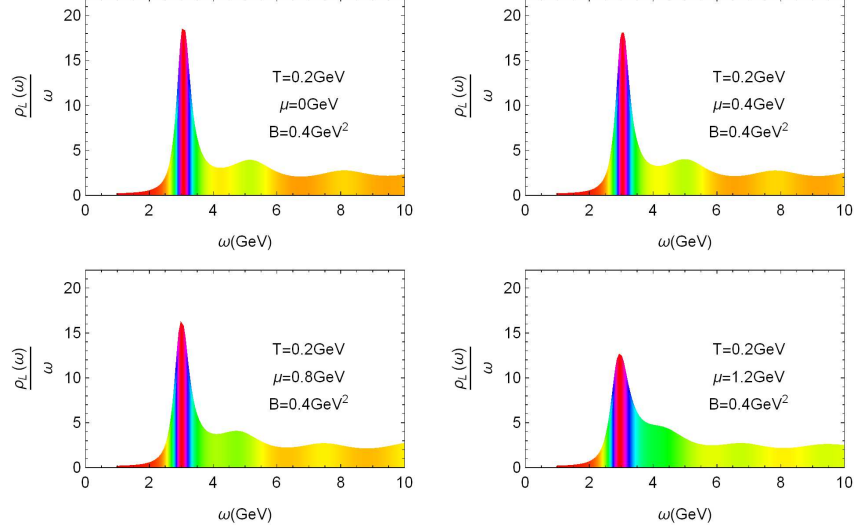


FIG. 6. The spectral functions of the  $J/\Psi$  state with different chemical potential  $\mu$  at  $T = 0.2 \text{ GeV}$  and  $B = 0.4 \text{ GeV}^2$ . From left to right and from top to bottom, the values of the chemical potential are  $\mu = 0 \text{ GeV}$ ,  $\mu = 0.4 \text{ GeV}$ ,  $\mu = 0.8 \text{ GeV}$  and  $\mu = 1.2 \text{ GeV}$  respectively.

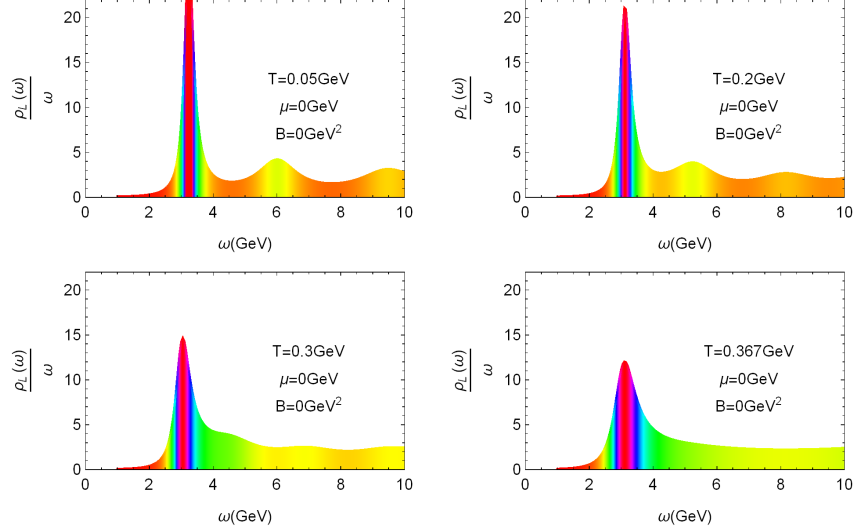


FIG. 7. The spectral functions of the  $J/\Psi$  state for different temperature  $T$  at  $\mu = 0 \text{ GeV}$  and  $B = 0 \text{ GeV}^2$ . From left to right and from top to bottom, the temperature are  $T = 0.05 \text{ GeV}$ ,  $T = 0.2 \text{ GeV}$ ,  $T = 0.3 \text{ GeV}$  and  $T = 0.367 \text{ GeV}$  respectively.

rapidly. Most notably, the peak will vanish when  $T > T_{max} = 0.367 \text{ GeV}$ . Of course, the maximum,  $T_{max}$ , decreases with the magnetic field and chemical potential. To summarize, the higher the temperature, the faster the  $J/\Psi$  state dissolves. Above we show the polarization parallel to the magnetic field, next we display the same figure for the polarization perpendicular to the

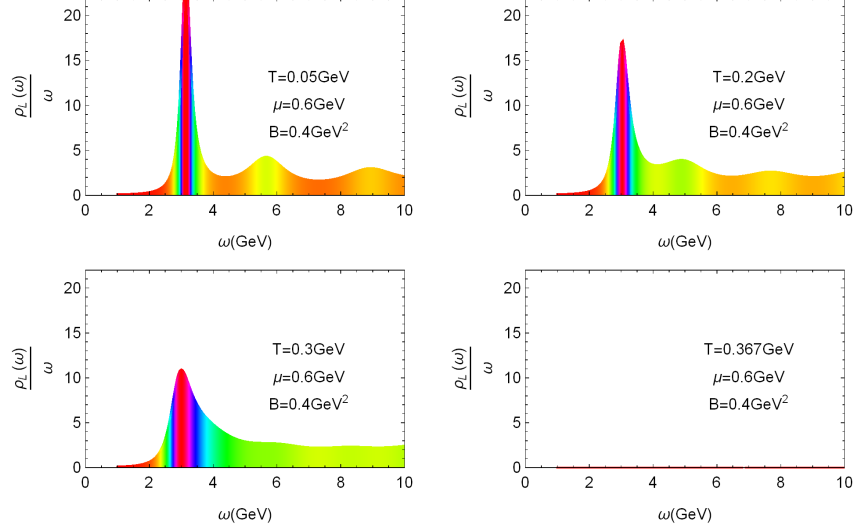


FIG. 8. The spectral functions of the  $J/\Psi$  state for different temperature  $T$  at  $\mu = 0.6 \text{ GeV}$  and  $B = 0.4 \text{ GeV}^2$ . From left to right and from top to bottom, the temperature are  $T = 0.05 \text{ GeV}$ ,  $T = 0.2 \text{ GeV}$ ,  $T = 0.3 \text{ GeV}$  and  $T = 0.367 \text{ GeV}$  respectively.

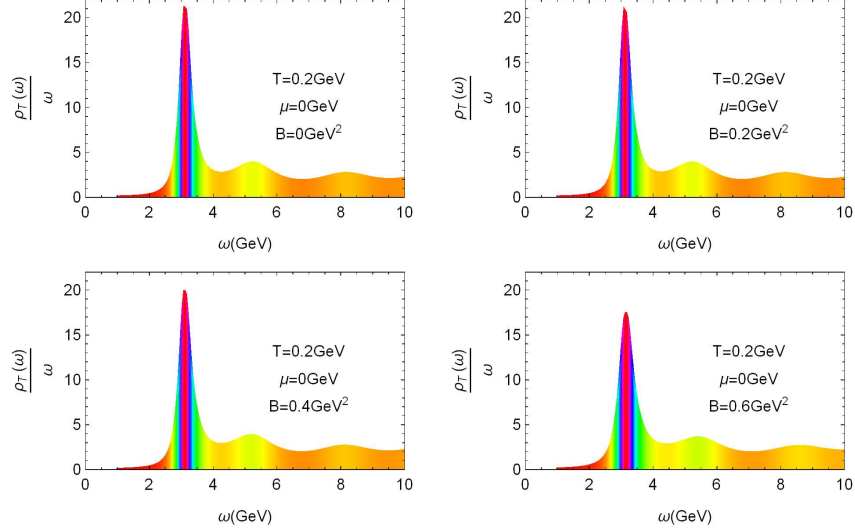


FIG. 9. The spectral functions of the  $J/\Psi$  state with different magnetic field  $B$  at  $T = 0.2 \text{ GeV}$  and  $\mu = 0 \text{ GeV}$ . From left to right and from top to bottom, the values of the magnetic field are  $B = 0 \text{ GeV}^2$ ,  $B = 0.2 \text{ GeV}^2$ ,  $B = 0.4 \text{ GeV}^2$  and  $B = 0.6 \text{ GeV}^2$  respectively.

magnetic field in Fig.9, Fig.10, Fig.11 and Fig.12. The conclusion for perpendicular cases of  $J/\Psi$  state are in line with the polarization parallel to the magnetic field. Comparison shows that the melting effect produced by the magnetic field is stronger when it is parallel to the polarization direction, which diametrically opposes to Ref.[48]. This difference comes from two aspects: One

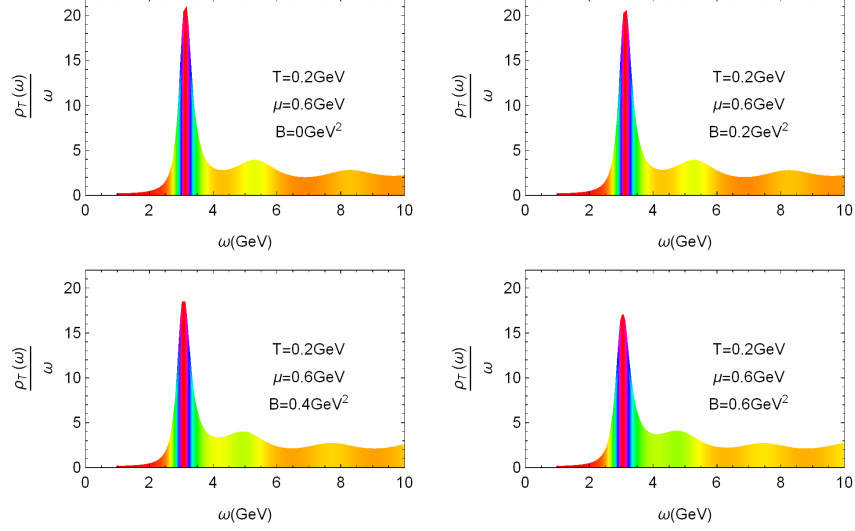


FIG. 10. The spectral functions of the  $J/\Psi$  state with different magnetic field  $B$  at  $T = 0.2\text{GeV}$  and  $\mu = 0.6\text{GeV}$ . From left to right and from top to bottom, the values of the magnetic field are  $B = 0\text{GeV}^2$ ,  $B = 0.2\text{GeV}^2$ ,  $B = 0.4\text{GeV}^2$  and  $B = 0.6\text{GeV}^2$  respectively.

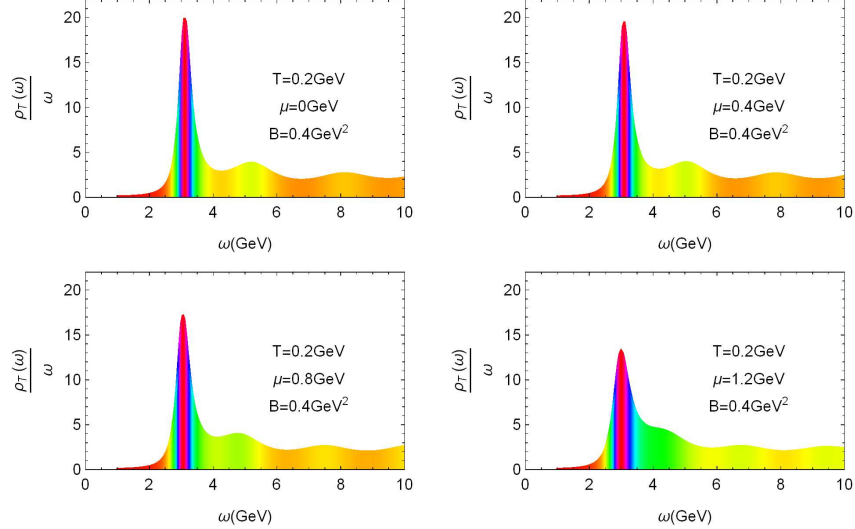


FIG. 11. The spectral functions of the  $J/\Psi$  state with different chemical potential  $\mu$  at  $T = 0.2\text{GeV}$  and  $B = 0.4\text{GeV}^2$ . From left to right and from top to bottom, the values of the chemical potential are  $\mu = 0\text{GeV}$ ,  $\mu = 0.4\text{GeV}$ ,  $\mu = 0.8\text{GeV}$  and  $\mu = 1.2\text{GeV}$  respectively.

is this result can be well explained by comparing Eq.(18) and Eq.(19) in terms of appearance, the appearance of the magnetic field in the denominator of the first term on the right of Eq. (18) and the molecule inside the bracket both decreases the value of  $Re \sigma$  numerically. In contrast, Eq.(19) does not have a magnetic field, formally. The second is the dilaton introduced in the action, in

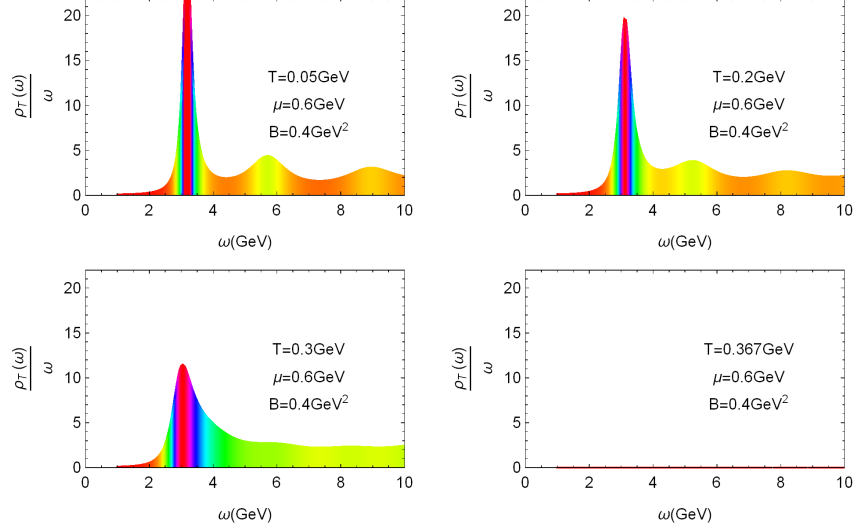


FIG. 12. The spectral functions of the  $J/\Psi$  state for different temperature  $T$  at  $\mu = 0.6\text{GeV}$  and  $B = 0.4\text{GeV}^2$ . From left to right and from top to bottom, the temperature are  $T = 0.05\text{GeV}$ ,  $T = 0.2\text{GeV}$ ,  $T = 0.3\text{GeV}$  and  $T = 0.367\text{GeV}$  respectively.

other words, that is the difference between EM model and EMD model. In this paper, we consider the EMD model. The advantages of EMD model can be found in Ref. [54]. The dilaton will deform the space and influence the magnetic field at different directions. Further, we find EMD model can realize the Cornell potential and show the magnetic field in parallel direction has large influence on potential. An action without the dilaton field cannot get a proper behavior of single quark. The result from lattice [66] also highlights the importance of a dilaton field in action.

In appendix , the spectral functions for  $\Upsilon(1S)$  state with various cases are shown Fig. 13- 22. Like  $J/\Psi$  state, the increasing temperature, chemical potential and magnetic field all decrease the height of the peak of spectral functions for  $\Upsilon(1S)$  state. One thing we have to pay attention to is that chemical potential significantly reduces the height of spectral functions peak for  $\Upsilon(1S)$  in zero magnetic field, which is different from  $J/\Psi$ . The influence produced by chemical potential is stronger with the increase of the mass of heavy meson.

## V. SUMMARY AND DISCUSS

In this paper, we draw support from a general, magnetic field dependent gravity to investigate the spectral functions of heavy mesons( $J/\Psi$  and  $\Upsilon(1S)$ ). Here, the heavy vector mesons are represented by a phenomenological model proposed in Ref. [59]. The spectral functions are cal-

culated by using membrane paradigm [63]. The results show that increasing chemical potential, magnetic field and temperature all reduce the height of the spectral functions peak, which means boosting heavy meson melting. The behavior of spectral functions is extraordinarily sensitive to temperature. With the increase of QGP temperature, the height of peak decreases rapidly. Most notably, the peak, representing the  $J/\Psi$  state, will vanish showing the formation of free quarks when  $T > T_{max}(B|_{=0}, \mu|_{=0}) = 0.367 GeV \approx 1.4T_c$ , which is consistent with the conclusion of lattice [1]. They pointed out the dissociation temperatures in the charmonium system is between  $1.1T_c$ (from  $F$  ansatz) and  $2.0T_c$ (from  $U$  ansatz). There is an interesting phenomenon, when the magnetic field does not exist, the chemical potential has little effect on the melting of  $J/\Psi$  state, but has a great influence on  $\Upsilon(1S)$ . However, when the magnetic field exist, the chemical potential has a significant effect on both  $J/\Psi$  state and  $\Upsilon(1S)$  state melting. In future work, we maybe investigate the thermodynamic properties of QGP and heavy meson melting by constructing a non-quadratic dilaton field. The results show that the suppression of the heavy meson is stronger with the increase of mass of heavy meson. In addition, in our holographic model, a dilaton field is introduced and we assume the magnetic field only affects the geometry perpendicular to the magnetic field, which leads to the magnetic field has a stronger effect on heavy mesons melting when it is parallel to the polarization.

## ACKNOWLEDGMENTS

This work is supported by the National Natural Science Foundation of China by Grant Nos. 11735007, 11890711, and 11890710.

## Appendix A: The spectral functions for $\Upsilon(1S)$ state

Fig. 13- 22 show the spectral functions for  $\Upsilon(1S)$  state in the polarization perpendicular to the magnetic field and parallel cases.

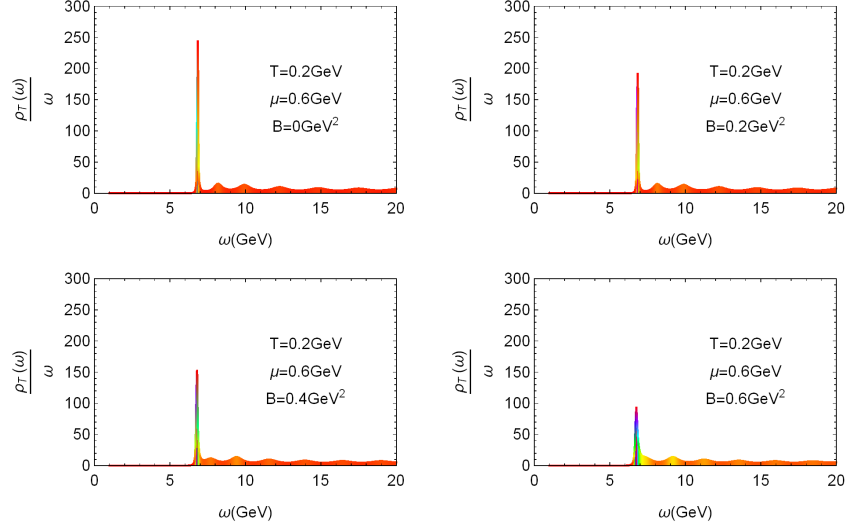


FIG. 14. The spectral functions of the  $\Upsilon(1S)$  state with different magnetic field  $B$  at  $T = 0.2\text{GeV}$  and  $\mu = 0.6\text{GeV}$ . From left to right and from top to bottom, the values of the magnetic field are  $B = 0\text{GeV}^2$ ,  $B = 0.2\text{GeV}^2$ ,  $B = 0.4\text{GeV}^2$  and  $B = 0.6\text{GeV}^2$  respectively.

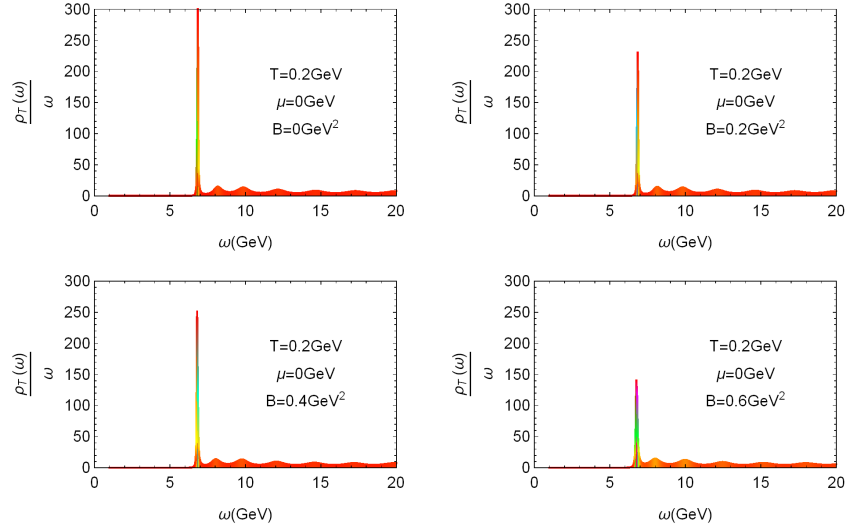


FIG. 13. The spectral functions of the  $\Upsilon(1S)$  state with different magnetic field  $B$  at  $T = 0.2\text{GeV}$  and  $\mu = 0\text{GeV}$ . From left to right and from top to bottom, the values of the magnetic field are  $B = 0\text{GeV}^2$ ,  $B = 0.2\text{GeV}^2$ ,  $B = 0.4\text{GeV}^2$  and  $B = 0.6\text{GeV}^2$  respectively.

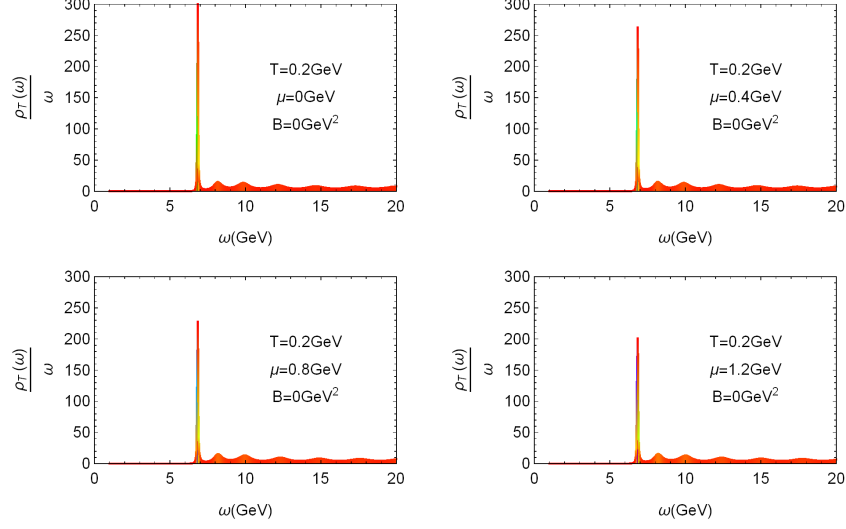


FIG. 15. The spectral functions of the  $\Upsilon(1S)$  state with different chemical potential  $\mu$  at  $T = 0.2\text{GeV}$  and  $B = 0\text{GeV}^2$ . From left to right and from top to bottom, the values of the chemical potential are  $\mu = 0\text{GeV}$ ,  $\mu = 0.4\text{GeV}$ ,  $\mu = 0.8\text{GeV}$  and  $\mu = 1.2\text{GeV}$  respectively.

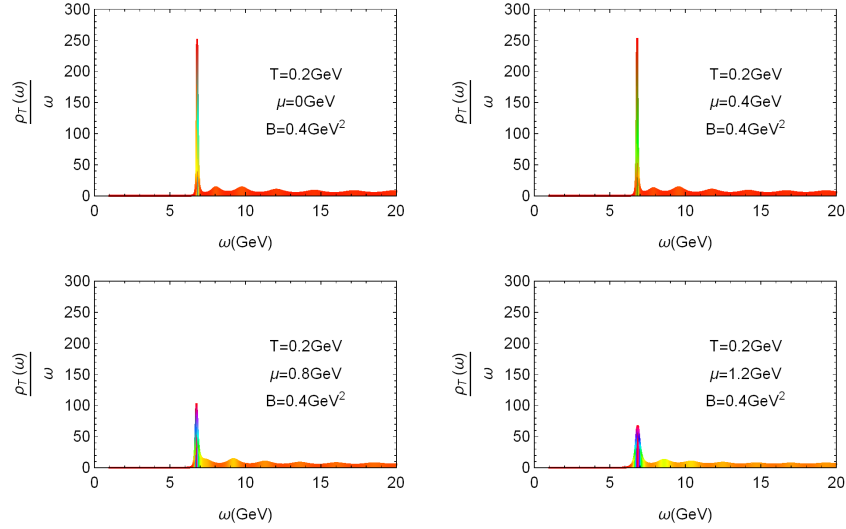


FIG. 16. The spectral functions of the  $\Upsilon(1S)$  state with different chemical potential  $\mu$  at  $T = 0.2\text{GeV}$  and  $B = 0.4\text{GeV}^2$ . From left to right and from top to bottom, the values of the chemical potential are  $\mu = 0\text{GeV}$ ,  $\mu = 0.4\text{GeV}$ ,  $\mu = 0.8\text{GeV}$  and  $\mu = 1.2\text{GeV}$  respectively.



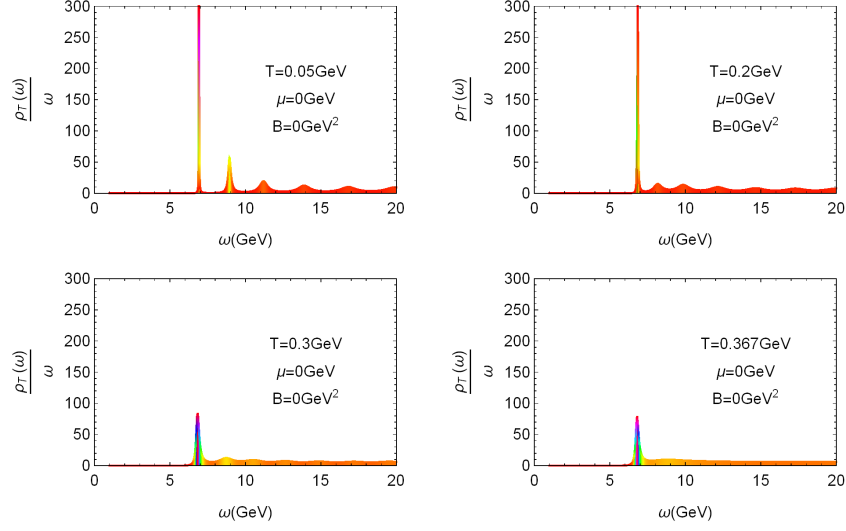


FIG. 17. The spectral functions of the  $\Upsilon(1S)$  state for different temperature  $T$  at  $\mu = 0 \text{ GeV}$  and  $B = 0 \text{ GeV}^2$ . From left to right and from top to bottom, the temperature are  $T = 0.05 \text{ GeV}$ ,  $T = 0.2 \text{ GeV}$ ,  $T = 0.3 \text{ GeV}$  and  $T = 0.367 \text{ GeV}$  respectively.

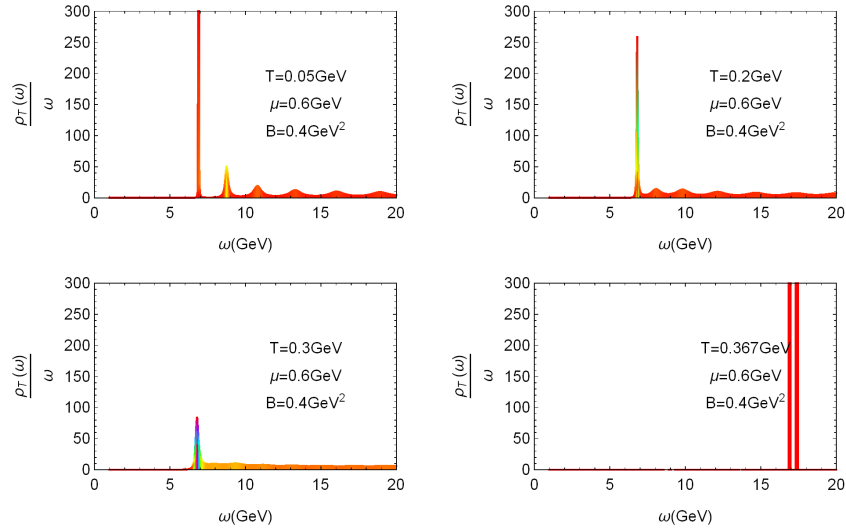


FIG. 18. The spectral functions of the  $\Upsilon(1S)$  state for different temperature  $T$  at  $\mu = 0.6 \text{ GeV}$  and  $B = 0.4 \text{ GeV}^2$ . From left to right and from top to bottom, the temperature are  $T = 0.05 \text{ GeV}$ ,  $T = 0.2 \text{ GeV}$ ,  $T = 0.3 \text{ GeV}$  and  $T = 0.367 \text{ GeV}$  respectively.

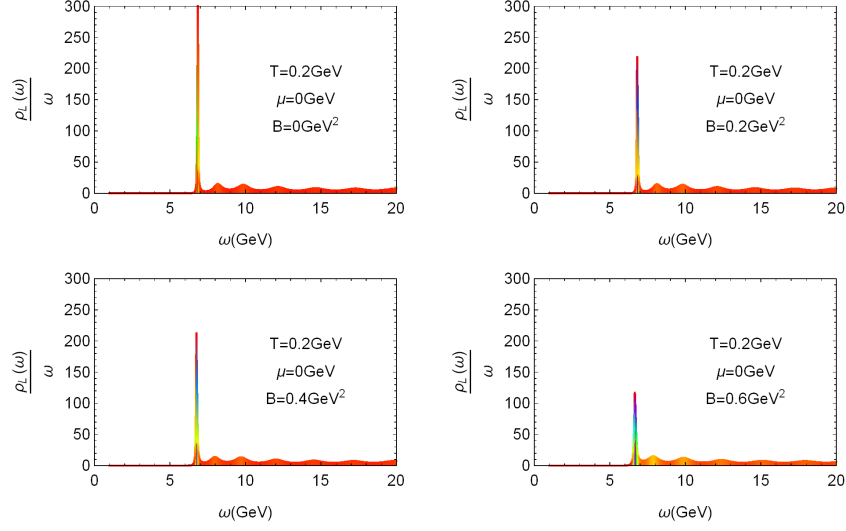


FIG. 19. The spectral functions of the  $\Upsilon(1S)$  state with different magnetic field  $B$  at  $T = 0.2\text{GeV}$  and  $\mu = 0\text{GeV}$ . From left to right and from top to bottom, the values of the magnetic field are  $B = 0\text{GeV}^2$ ,  $B = 0.2\text{GeV}^2$ ,  $B = 0.4\text{GeV}^2$  and  $B = 0.6\text{GeV}^2$  respectively.

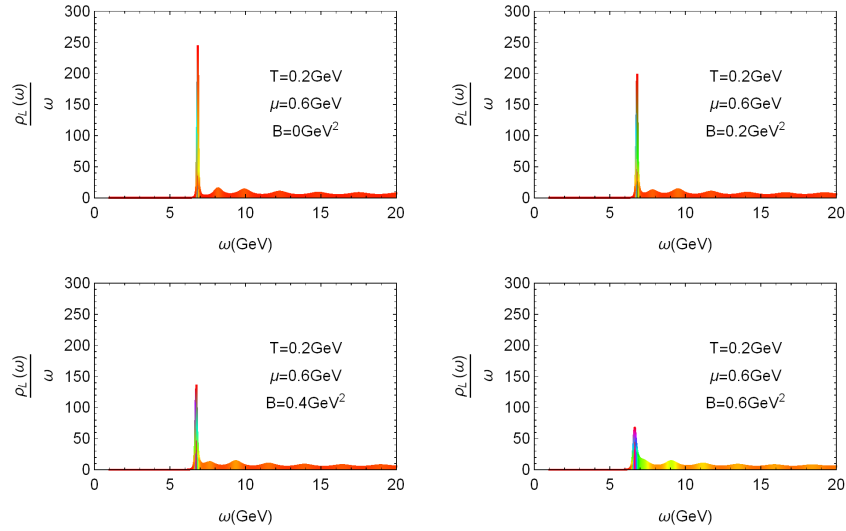


FIG. 20. The spectral functions of the  $\Upsilon(1S)$  state with different magnetic field  $B$  at  $T = 0.2\text{GeV}$  and  $\mu = 0.6\text{GeV}$ . From left to right and from top to bottom, the values of the magnetic field are  $B = 0\text{GeV}^2$ ,  $B = 0.2\text{GeV}^2$ ,  $B = 0.4\text{GeV}^2$  and  $B = 0.6\text{GeV}^2$  respectively.

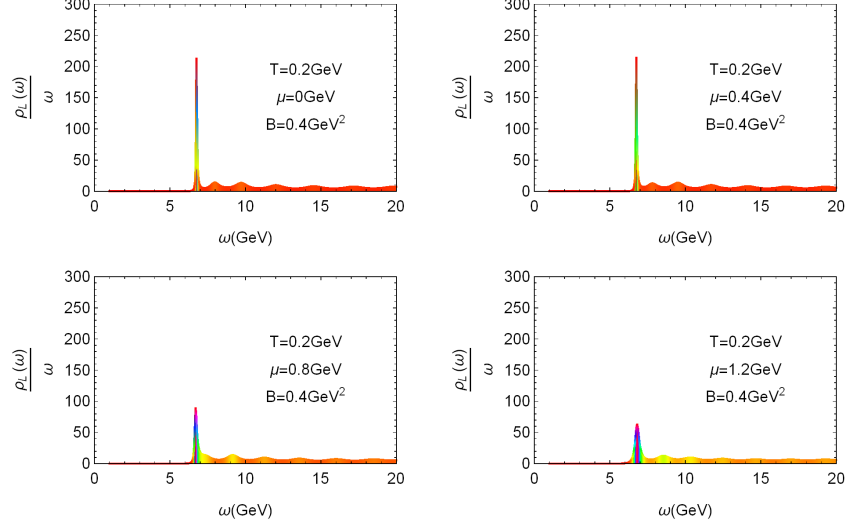


FIG. 21. The spectral functions of the  $\Upsilon(1S)$  state with different chemical potential  $\mu$  at  $T = 0.2\text{GeV}$  and  $B = 0.4\text{GeV}^2$ . From left to right and from top to bottom, the values of the chemical potential are  $\mu = 0\text{GeV}$ ,  $\mu = 0.4\text{GeV}$ ,  $\mu = 0.8\text{GeV}$  and  $\mu = 1.2\text{GeV}$  respectively.

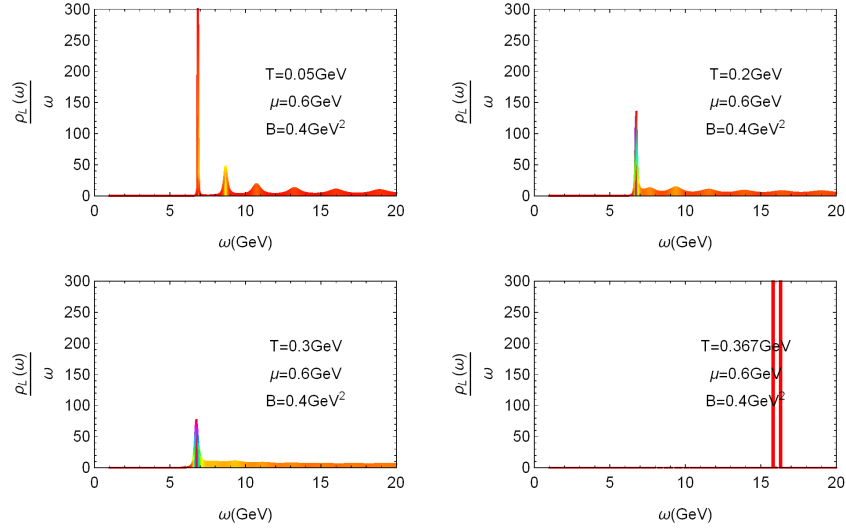


FIG. 22. The spectral functions of the  $\Upsilon(1S)$  state for different temperature  $T$  at  $\mu = 0.6\text{GeV}$  and  $B = 0.4\text{GeV}^2$ . From left to right and from top to bottom, the temperature are  $T = 0.05\text{GeV}$ ,  $T = 0.2\text{GeV}$ ,  $T = 0.3\text{GeV}$  and  $T = 0.367\text{GeV}$  respectively.

- 
- [1] Frithjof Karsch. Deconfinement and quarkonium suppression. *Eur. Phys. J. C*, 43:35–43, 2005.
- [2] Miklos Gyulassy and Larry McLerran. New forms of QCD matter discovered at RHIC. *Nucl. Phys. A*, 750:30–63, 2005.
- [3] Juan Martin Maldacena. The Large N limit of superconformal field theories and supergravity. *Adv. Theor. Math. Phys.*, 2:231–252, 1998.
- [4] Edward Witten. Anti-de Sitter space and holography. *Adv. Theor. Math. Phys.*, 2:253–291, 1998.
- [5] Sebastian de Haro, Sergey N. Solodukhin, and Kostas Skenderis. Holographic reconstruction of space-time and renormalization in the AdS / CFT correspondence. *Commun. Math. Phys.*, 217:595–622, 2001.
- [6] Soo-Jong Rey and Jung-Tay Yee. Macroscopic strings as heavy quarks in large N gauge theory and anti-de Sitter supergravity. *Eur. Phys. J. C*, 22:379–394, 2001.
- [7] Igor R. Klebanov and Edward Witten. AdS / CFT correspondence and symmetry breaking. *Nucl. Phys. B*, 556:89–114, 1999.
- [8] Andreas Karch and Emanuel Katz. Adding flavor to AdS / CFT. *JHEP*, 06:043, 2002.
- [9] Joshua Erlich, Emanuel Katz, Dam T. Son, and Mikhail A. Stephanov. QCD and a holographic model of hadrons. *Phys. Rev. Lett.*, 95:261602, 2005.
- [10] Daniel Z. Freedman, Samir D. Mathur, Alec Matusis, and Leonardo Rastelli. Correlation functions in the CFT(d) / AdS(d+1) correspondence. *Nucl. Phys. B*, 546:96–118, 1999.
- [11] Giuseppe Policastro, Dam T. Son, and Andrei O. Starinets. From AdS / CFT correspondence to hydrodynamics. *JHEP*, 09:043, 2002.
- [12] Jorge Casalderrey-Solana, Hong Liu, David Mateos, Krishna Rajagopal, and Urs Achim Wiedemann. *Gauge/String Duality, Hot QCD and Heavy Ion Collisions*. Cambridge University Press, 2014.
- [13] Rajesh Gopakumar and Cumrun Vafa. On the gauge theory / geometry correspondence. *Adv. Theor. Math. Phys.*, 3:1415–1443, 1999.
- [14] Roberto Emparan, Clifford V. Johnson, and Robert C. Myers. Surface terms as counterterms in the AdS / CFT correspondence. *Phys. Rev. D*, 60:104001, 1999.
- [15] Marco M. Caldarelli, Guido Cognola, and Dietmar Klemm. Thermodynamics of Kerr-Newman-AdS black holes and conformal field theories. *Class. Quant. Grav.*, 17:399–420, 2000.

- [16] S. W. Hawking, C. J. Hunter, and Marika Taylor. Rotation and the AdS / CFT correspondence. *Phys. Rev. D*, 59:064005, 1999.
- [17] T. Hatsuda and T. Kunihiro. Fluctuation Effects in Hot Quark Matter: Precursors of Chiral Transition at Finite Temperature. *Phys. Rev. Lett.*, 55:158–161, 1985.
- [18] M. Asakawa and T. Hatsuda. J / psi and eta(c) in the deconfined plasma from lattice QCD. *Phys. Rev. Lett.*, 92:012001, 2004.
- [19] Saumen Datta, Frithjof Karsch, Peter Petreczky, and Ines Wetzorke. Behavior of charmonium systems after deconfinement. *Phys. Rev. D*, 69:094507, 2004.
- [20] V. Skokov, A. Yu. Illarionov, and V. Toneev. Estimate of the magnetic field strength in heavy-ion collisions. *Int. J. Mod. Phys. A*, 24:5925–5932, 2009.
- [21] Adam Bzdak and Vladimir Skokov. Event-by-event fluctuations of magnetic and electric fields in heavy ion collisions. *Phys. Lett. B*, 710:171–174, 2012.
- [22] Zhou-Run Zhu, De-fu Hou, and Xun Chen. Potential analysis of holographic Schwinger effect in the magnetized background. *Eur. Phys. J. C*, 80(6):550, 2020.
- [23] Zhou-Run Zhu, Yang-Kang Liu, and Defu Hou. Holographic Schwinger effect in the dynamical AdS/QCD model. 8 2021.
- [24] V. Voronyuk, V. D. Toneev, W. Cassing, E. L. Bratkovskaya, V. P. Konchakovski, and S. A. Voloshin. (Electro-)Magnetic field evolution in relativistic heavy-ion collisions. *Phys. Rev. C*, 83:054911, 2011.
- [25] Victor Roy, Shi Pu, Luciano Rezzolla, and Dirk H. Rischke. Effect of intense magnetic fields on reduced-MHD evolution in  $\sqrt{s_{NN}} = 200$  GeV Au+Au collisions. *Phys. Rev. C*, 96(5):054909, 2017.
- [26] Kirill Tuchin. Particle production in strong electromagnetic fields in relativistic heavy-ion collisions. *Adv. High Energy Phys.*, 2013:490495, 2013.
- [27] N. Seiberg. Electric - magnetic duality in supersymmetric nonAbelian gauge theories. *Nucl. Phys. B*, 435:129–146, 1995.
- [28] V. P. Gusynin, V. A. Miransky, and I. A. Shovkovy. Dimensional reduction and catalysis of dynamical symmetry breaking by a magnetic field. *Nucl. Phys. B*, 462:249–290, 1996.
- [29] Dmitri E. Kharzeev and Ho-Ung Yee. Chiral Magnetic Wave. *Phys. Rev. D*, 83:085007, 2011.
- [30] Florian Preis, Anton Rebhan, and Andreas Schmitt. Inverse magnetic catalysis in dense holographic matter. *JHEP*, 03:033, 2011.
- [31] Tameem Albash, Veselin G. Filev, Clifford V. Johnson, and Arnab Kundu. Finite temperature large N gauge theory with quarks in an external magnetic field. *JHEP*, 07:080, 2008.

- [32] Tigran Kalaydzhyan and Ingo Kirsch. Fluid/gravity model for the chiral magnetic effect. *Phys. Rev. Lett.*, 106:211601, 2011.
- [33] Stefano Ivo Finazzo, Renato Critelli, Romulo Rougemont, and Jorge Noronha. Momentum transport in strongly coupled anisotropic plasmas in the presence of strong magnetic fields. *Phys. Rev. D*, 94(5):054020, 2016. [Erratum: *Phys.Rev.D* 96, 019903 (2017)].
- [34] Florian Preis, Anton Rebhan, and Andreas Schmitt. Inverse magnetic catalysis in field theory and gauge-gravity duality. *Lect. Notes Phys.*, 871:51–86, 2013.
- [35] Romulo Rougemont, Renato Critelli, and Jorge Noronha. Holographic calculation of the QCD crossover temperature in a magnetic field. *Phys. Rev. D*, 93(4):045013, 2016.
- [36] Yan-Yan Bu, Johanna Erdmenger, Jonathan P. Shock, and Migael Strydom. Magnetic field induced lattice ground states from holography. *JHEP*, 03:165, 2013.
- [37] Carlos Hoyos, Tatsuma Nishioka, and Andy O’Bannon. A Chiral Magnetic Effect from AdS/CFT with Flavor. *JHEP*, 10:084, 2011.
- [38] A. Gorsky, P. N. Kopnin, and A. V. Zayakin. On the Chiral Magnetic Effect in Soft-Wall AdS/QCD. *Phys. Rev. D*, 83:014023, 2011.
- [39] Rong-Gen Cai, Song He, Li Li, and Li-Fang Li. A Holographic Study on Vector Condensate Induced by a Magnetic Field. *JHEP*, 12:036, 2013.
- [40] Kiminad A. Mamo. Inverse magnetic catalysis in holographic models of QCD. *JHEP*, 05:121, 2015.
- [41] Kristan Jensen, Andreas Karch, and Ethan G. Thompson. A Holographic Quantum Critical Point at Finite Magnetic Field and Finite Density. *JHEP*, 05:015, 2010.
- [42] D. Dudal, Diego R. Granado, and Thomas G. Mertens. No inverse magnetic catalysis in the QCD hard and soft wall models. *Phys. Rev. D*, 93(12):125004, 2016.
- [43] Niko Jokela, Gilad Lifschytz, and Matthew Lippert. Magnetic effects in a holographic Fermi-like liquid. *JHEP*, 05:105, 2012.
- [44] N. Callebaut, D. Dudal, and H. Verschelde. Holographic rho mesons in an external magnetic field. *JHEP*, 03:033, 2013.
- [45] Veselin G. Filev and Radoslav C. Raskov. Magnetic Catalysis of Chiral Symmetry Breaking. A Holographic Prospective. *Adv. High Energy Phys.*, 2010:473206, 2010.
- [46] Umut Gürsoy, Ioannis Iatrakis, Matti Järvinen, and Govert Nijs. Inverse Magnetic Catalysis from improved Holographic QCD in the Veneziano limit. *JHEP*, 03:053, 2017.

- [47] Nick Evans, Carlisson Miller, and Marc Scott. Inverse Magnetic Catalysis in Bottom-Up Holographic QCD. *Phys. Rev. D*, 94(7):074034, 2016.
- [48] Nelson R. F. Braga and Luiz F. Ferreira. Heavy meson dissociation in a plasma with magnetic fields. *Phys. Lett. B*, 783:186–192, 2018.
- [49] Pietro Colangelo, Floriana Giannuzzi, Stefano Nicotri, and Fen Zuo. Temperature and chemical potential dependence of the gluon condensate: a holographic study. *Phys. Rev. D*, 88(11):115011, 2013.
- [50] Umut Gursoy, Matti Jarvinen, and Govert Nijs. Holographic QCD in the Veneziano Limit at a Finite Magnetic Field and Chemical Potential. *Phys. Rev. Lett.*, 120(24):242002, 2018.
- [51] Nelson R. F. Braga and Luiz F. Ferreira. Quasinormal modes for quarkonium in a plasma with magnetic fields. *Phys. Lett. B*, 795:462–468, 2019.
- [52] Zhou-Run Zhu, Sheng-Qin Feng, Ya-Fei Shi, and Yang Zhong. Energy loss of heavy and light quarks in holographic magnetized background. *Phys. Rev. D*, 99(12):126001, 2019.
- [53] Danning Li, Mei Huang, Yi Yang, and Pei-Hung Yuan. Inverse Magnetic Catalysis in the Soft-Wall Model of AdS/QCD. *JHEP*, 02:030, 2017.
- [54] Jing Zhou, Xun Chen, Yan-Qing Zhao, and Jialun Ping. Thermodynamics of heavy quarkonium in a magnetic field background. *Phys. Rev. D*, 102(8):086020, 2020.
- [55] Sheng-Qin Feng, Yan-Qing Zhao, and Xun Chen. Systematical study of thermal width of heavy quarkonia in a finite temperature magnetized background from holography. *Phys. Rev. D*, 101(2):026023, 2020.
- [56] Mitsutoshi Fujita, Kenji Fukushima, Tatsuhiro Misumi, and Masaki Murata. Finite-temperature spectral function of the vector mesons in an AdS/QCD model. *Phys. Rev. D*, 80:035001, 2009.
- [57] T. Umeda, R. Katayama, O. Miyamura, and H. Matsufuru. Study of charmonia near the deconfining transition on an anisotropic lattice with O(a) improved quark action. *Int. J. Mod. Phys. A*, 16:2215, 2001.
- [58] Daniel Ávila and Leonardo Patiño. Melting holographic mesons by cooling a magnetized quark gluon plasma. *JHEP*, 06:010, 2020.
- [59] Nelson R. F. Braga, Luiz F. Ferreira, and Alfredo Vega. Holographic model for charmonium dissociation. *Phys. Lett. B*, 774:476–481, 2017.
- [60] Defu Hou and Hai-cang Ren. Heavy Quarkonium States with the Holographic Potential. *JHEP*, 01:029, 2008.

- [61] Hardik Bohra, David Dudal, Ali Hajilou, and Subhash Mahapatra. Anisotropic string tensions and inversely magnetic catalyzed deconfinement from a dynamical AdS/QCD model. *Phys. Lett. B*, 801:135184, 2020.
- [62] David Dudal and Subhash Mahapatra. Thermal entropy of a quark-antiquark pair above and below deconfinement from a dynamical holographic QCD model. *Phys. Rev. D*, 96(12):126010, 2017.
- [63] Nabil Iqbal and Hong Liu. Universality of the hydrodynamic limit in AdS/CFT and the membrane paradigm. *Phys. Rev. D*, 79:025023, 2009.
- [64] M. Tanabashi et al. Review of Particle Physics. *Phys. Rev. D*, 98(3):030001, 2018.
- [65] Miguel Angel Martin Contreras, Saulo Diles, and Alfredo Vega. Heavy quarkonia spectroscopy at zero and finite temperature in bottom-up AdS/QCD. *Phys. Rev. D*, 103(8):086008, 2021.
- [66] Claudio Bonati, Massimo D’Elia, Marco Mariti, Michele Mesiti, Francesco Negro, Andrea Rucci, and Francesco Sanfilippo. Magnetic field effects on the static quark potential at zero and finite temperature. *Phys. Rev. D*, 94(9):094007, 2016.